Mössbauer and Electron Paramagnetic Resonance Studies of Horseradish Peroxidase and Its Catalytic Intermediates†

C. E. Schulz,‡ R. Rutter,§ J. T. Sage, P. G. Debrunner,* and L. P. Hager

ABSTRACT: We report Mössbauer and EPR measurements on horseradish peroxidase in the native state and the reaction intermediates with peroxide and chlorite. A detailed analysis of the electronic state of the heme iron is given, and comparisons are drawn with related systems. The native enzyme is high-spin ferric and thus has three Kramers doublets. The unusual magnetic properties of the ground doublet and the large energy of the second, $(E_2 - E_1)/k \approx 41$ K, and third doublet, $(E_3 - E_1)/k \gtrsim 170$ K, can be modeled with a quartet admixture of ~11% to the spin sextet. All evidence suggests a ferryl, OFe^{IV}, state of the heme iron in compounds I and II and related complexes. The small isomer shift, $\delta_{Fe} \approx 0.06$ mm/s, the (positive) quadrupole splitting, $\Delta E_Q \approx 1.4$ mm/s, the spin $S = 1$, and the large positive zero field splitting, $D/k \approx 35$ K, are all characteristic of the ferryl state. In the green compound I the iron weakly couples to a porphyrin radical with spin $S' = {}^1/_2$. A phenomenological model with a weak exchange interaction $\tilde{S}\cdot\mathbf{J}\cdot\tilde{S}'$, $|J| \lesssim 0.1$ D, reproduces all Mössbauer and EPR data of compound I, but the structural origin of the exchange and its apparent distribution require further study. Reaction of horseradish peroxidase with chlorite leads to compound X with $\delta_{Fe} = 0.07$ mm/s and $\Delta E_Q = 1.53$ mm/s, values that are closest to those of compound II. The diamagnetism of compound III and its Mössbauer parameters $\delta_{Fe} = 0.23$ mm/s and $\Delta E_Q = -2.31$ mm/s at 4.2 K clearly identify it as an oxyheme adduct.

Ever since its discovery and isolation, horseradish peroxidase has provided enzymologists and protein chemists with a rich source of material for experimental observation (Willstätter & Stoll, 1918; Willstätter & Pollinger, 1923). Horseradish peroxidase attracted much attention in its early years because of its plentiful supply and ease of purification (Theorell, 1942). The subsequent discovery of oxidized enzyme intermediates during peroxidative catalysis by horseradish peroxidase was the first direct detection of the formation of an enzyme intermediate. This discovery triggered a burst of activity aimed at the chemical characterization of the native and oxidized forms of the enzyme. Horseradish peroxidase compound II was soon recognized as an oxidized enzyme intermediate that contained 1 additional oxidizing equiv over and above the native ferric resting form of the enzyme (Keilin & Mann, 1937). Horseradish peroxidase compound I was later identified as the green intermediate, which contains both of the oxidizing equivalents originally associated with the peroxide substrate prior to its reaction with the enzyme (Theorell, 1941). In the intervening years between the discovery of these compounds and the present time, the precise structure of these enzyme intermediates has been sharply debated and investigated. Recently, a general consensus has emerged with respect to compounds I and II. For the most part, this agreement had to await the development and application of more sophisticated physical techniques for probing heme–protein structures. These physical approaches coupled with chemical models and isotopic oxygen analyses now provide a sound experimental and theoretical framework for a molecular description of the events occurring at the heme active site of horseradish peroxidase during enzyme catalysis.

In this paper we analyze the electronic environment of the heme iron atom in the native enzyme and in horseradish peroxidase compounds I–III and X. Our Mössbauer and EPR results are consistent with the native enzyme containing a ferric iron having five unpaired 3d electrons, with compound I being a ferryl porphyrin π-cation radical, with compound II and compound X containing the ferryl structure, and with compound III being an O_2 adduct of ferrous horseradish peroxidase (HRP).

Materials and Methods

Hydrogen peroxide was obtained from Fischer Scientific Co. and assayed by the method of Cotton et al. (1973). Glycerol from the same source was vacuum distilled prior to use in order to remove any oxidizable compounds. Benzohydroxamic acid from Aldrich Chemical Co. was used without further purification. Horseradish peroxidase was obtained from Sigma Chemical Co. and purified by the method of Shannon et al. (1966) to an R_z value (A_{403nm}/A_{278nm}) ≥ 3.35. The concentrations of the HRP preparations were determined photometrically at 403 nm by using a molar absorptivity coefficient of 1.02×10^5 M^{-1} cm^{-1} (Schonbaum & Lo, 1972). All samples used for Mössbauer spectroscopy were enriched in ^{57}Fe by heme exchange.

[^{57}Fe]Protoporphyrin IX was prepared by the procedure of Adler et al. (1970) from the free acid form of protoporphyrin IX (Sigma Chemical Co.). The final ^{57}Fe-labeled product had a reduced pyridine hemochromogen spectrum with an absorbance ratio at 557 nm to 541 nm of 3.38. The substitution of [^{57}Fe]heme into apoperoxidase was accomplished by the methods of Tamura et al. (1972). After reconstitution, the holoenzyme was rechromatographed on a CM-52 resin according to the procedures used to purify HRP isozyme C (Shannon et al., 1966). For the preparation of the ^{57}Fe-labeled native sample, the HRP obtained in the previous step was dialyzed against a 1000-fold excess of 0.05 M potassium phosphate, pH 6.9, and was then concentrated to about 5 mM with a PM-10 membrane in a small Amicon ultrafiltration unit. Solid benzohydroxamic acid was added to the concentrated enzyme to produce an equimolar ratio of ligand to enzyme. The benzohydroxamic acid complex was brought to about 35% glycerol in order to form a good glass for low-temperature spectroscopy.

All compound I samples were prepared in water that had been purified first by deionization and then by triple distil-

† From the Departments of Physics and Biochemistry, University of Illinois at Urbana-Champaign, Urbana, Illinois 61801. *Received March 7, 1984.* Supported in part by Grants USPH GM16406 and GM07768.

‡ Present address: Department of Physics, Knox College, Galesburg, IL 61401.

§ Present address: Monsanto Co., St. Louis, MO 63167.

0006-2960/84/0423-4743$01.50/0

lation, once with potassium permanganate and twice by normal means. The purified native enzyme was first dialyzed against a 1000-fold excess of 0.05 M potassium phosphate, pH 6.9, and then concentrated to about 4 mM. Glycerol was added to the concentrated enzyme sample to a final concentration of 35%, and hydrogen peroxide was then added to give a molar ratio of hydrogen peroxide to enzyme of 1.2:1. A small aliquot of the compound I preparation was removed and its absorption spectrum (370–450 nm) was recorded on a Cary 219 spectrophotometer. Estimates of the relative amounts of compound I, compound II, and native enzyme were made by using the isosbestic points at 411 and 429 nm as reference standards. All compound I samples were at least 97% pure as judged from the spectral analysis. Preparations made according to this procedure were stable in millimolar concentrations for up to 3 h at room temperature and for up to 24 h in micromolar concentrations.

The spin standard, copper ethylenediaminetetraacetic acid (Cu-EDTA), was prepared by adding a 10-fold excess of EDTA (Sigma Chemical Co.) to a weighed sample of copper chloride (Alfa Products) and titrating the EDTA to its basic form with sodium hydroxide. Compound II was prepared by adding ascorbic acid to compound I to give a final molar ratio of 0.95 to 1. The admixture of compound I and native enzyme in these preparations was determined from the absorbance spectra as described above. All samples contained more than 90% compound II.

A 0.5 mM sample of compound X was prepared by addition of exactly 1.00 equiv of sodium chlorite to ^{57}Fe-enriched native horseradish peroxidase in carbonate buffer, pH 10.2 (Chiang et al., 1976; Shahangian & Hager, 1982). Under these conditions compound X took about 2 h to form, and it was stable at room temperature for a few days.

Compound III was prepared by adding a 100-fold molar excess of hydrogen peroxide to compound II in the concentration range of 0.5 mM. The resulting samples contained compound III and some impurity. At higher concentrations, the 100-fold excess of hydrogen peroxide tended to partially denature the enzyme.

For Mössbauer measurements, the samples were mounted in one of several cryostats, which allowed temperature variation from 2 to 300 K and application of magnetic fields up to 5.5 T. A 50-mCi source of ^{57}Co diffused into a rhodium foil was used (Amersham, England). Doppler shifts were calibrated with an iron foil at 300 K. The symmetry point of the iron spectrum was taken as a zero Doppler shift for all Mössbauer data reported in this paper.

Electron paramagnetic resonance (EPR) spectra were recorded on a Varian E9 or a Bruker ER200 X-band spectrometer with an Oxford Instruments helium-flow cryostat. This cryostat maintains a set sensor temperature within 0.1 K, but the actual sample temperature was found to correlate poorly with the set value.

Analysis of the Mössbauer and EPR Spectra. Except for the diamagnetic compound III, all states of HRP considered here are paramagnetic, and a spin-Hamiltonian model proved to be most efficient for the parametrization of the Mössbauer and EPR spectra. In this model, an effective spin S is assigned to the electronic ground state of the iron such that the multiplicity $(2S + 1)$ is the total number of sublevels into which this ground state can split. We assume that the splitting is given by the electronic Hamiltonian

$$\hat{\mathcal{H}}_e = D[\hat{S}_z^2 - S(S+1)/3] + E(\hat{S}_x^2 - \hat{S}_y^2) + \beta_e \vec{S}\cdot\mathbf{g}\cdot\vec{H} \quad (1)$$

where $\vec{S} = (\hat{S}_x, \hat{S}_y, \hat{S}_z)$ is the spin operator, the phenomenological parameters D and E describe the axial and rhombic zero field splitting, and the last term is the Zeeman interaction with an externally applied magnetic field $\vec{H}$. Further terms must be added to $\hat{\mathcal{H}}_e$ in order to describe compound I, which contains a free radical of spin $S' = {}^1/_2$ that couples to the spin $S = 1$ located on the heme iron:

$$\hat{\mathcal{H}}_e' = \beta_e g \vec{S}'\cdot\vec{H} + \vec{S}\cdot\mathbf{J}\cdot\vec{S}' \quad (2)$$

Here, $\mathbf{J}$ is a tensor that represents the spin–spin interaction; the isotropic term typically dominates (Moriya et al., 1960). Quite generally, a spin-Hamiltonian model is adequate if the energies of all excited orbital and spin states of the paramagnetic ion are much larger than the splittings given by $\hat{\mathcal{H}}_e$, $\hat{\mathcal{H}}_e'$, and the thermal energy kT. Even if these conditions are not satisfied, as appears to be the case for native horseradish peroxidase, a spin Hamiltonian may be used with appropriate corrections. The EPR spectra of the native enzyme and compound I can be parametrized by using eq 1 and 2 with a suitable model of the line shape. The model adopted assumes a Gaussian with an isotropic minimum width and furthermore allows a Gaussian distribution of the parameters about their mean values. Details are given in the Appendix.

In order to parametrize the Mössbauer spectra, eq 1 and 2 are combined with the nuclear Hamiltonian:

$$\hat{\mathcal{H}}_n = \vec{S}\cdot\mathbf{A}\cdot\vec{I} - \beta_n g_n \vec{I}\cdot\vec{H} + eQV_{zz}[3\hat{I}_z^2 - I(I+1) + \eta(\hat{I}_x^2 - \hat{I}_y^2)]/12 \quad (3)$$

Here, $\vec{I} = (\hat{I}_x, \hat{I}_y, \hat{I}_z)$ is the nuclear spin operator; the first term represents the magnetic hyperfine interaction of the nucleus with the spin $\vec{S}$ on the iron, the second term the nuclear Zeeman splitting, and the last term the electric quadrupole interaction $\hat{\mathcal{H}}_Q$ with the field gradient $-(V_{xx}, V_{yy}, V_{zz})$ arising from the local charge distribution. The asymmetry parameter η in $\hat{\mathcal{H}}_Q$ is defined as $\eta = (V_{xx} - V_{yy})/V_{zz}$. The experimentally observed quadrupole splitting is $\Delta E_Q = (1/2)eQV_{zz}(1 + \eta^2/3)^{1/2}$. Since the electronic spin $\vec{S}$ of the iron couples via spin–orbit interaction to the thermal vibrations of the protein, transitions take place between the eigenstates of eq 1 and 2, which may affect the shape of the Mössbauer spectra substantially. In the limit of slow spin fluctuation, typically encountered at low temperatures, the spectra may be calculated by assuming $\hat{\mathcal{H}}_e$ to be stationary and each energy level to be populated according to its Boltzmann factor. At higher temperatures, the opposite, fast-fluctuation limit applies, and a thermal average of the spin expectation value $\langle\vec{S}\rangle_T$ can be substituted in eq 3; in the absence of an applied field, $\langle\vec{S}\rangle_T$ is 0, and only quadrupole splitting is observed. The case of intermediate spin fluctuation, where the spin transition rate is comparable to nuclear Larmor frequencies, is treated by using the dynamical line-shape formalism of Blume & Clauser (1971). The model as elaborated by Winkler et al. (1979) assumes the spin transition rates to be dominated by direct and Orbach processes (Orbach & Stapleton, 1972). The lattice vibrations are approximated by the standard Debye model or a variation thereof, and a single adjustable rate parameter W_0 is introduced.

The formalism outlined above is used to simulate EPR (see Appendix) and Mössbauer spectra (Münck et al., 1973). The parameters are adjusted iteratively until a set is found that adequately reproduces all the data of a given state of HRP. The uniqueness of the resulting parametrizations has to be assessed for each individual compound. The meaning of the Hamiltonian parameters will be expanded upon under Discussion.

Results

Native Horseradish Peroxidase. All preparations of native enzyme showed an optical absorption characteristic of a

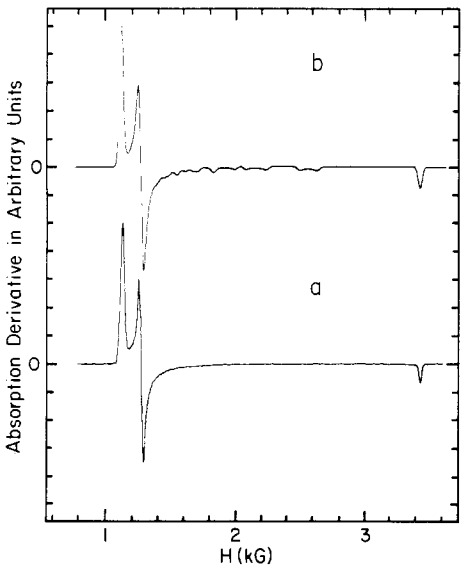

FIGURE 1: EPR spectrum of the benzohydroxamic acid complex of native enzyme. A 40% glycerol solution of 3 mM native HRP in 50 mM potassium phosphate, pH 6.5, was mixed with a 20% excess of benzohydroxamic acid. The lower trace (a) is the first derivative of the absorption signal as recorded at 3.8 K with 0.2-mW microwave power at 9.41 GHz and 100-kHz modulation of 1 mT. The upper trace (b) is a computer simulation performed with the program described in the Appendix. Parameters were chosen to best match the effective g tensor (6.10, 5.46, 1.98) as described under Results.

high-spin ferric heme protein at room temperature. The EPR spectra demonstrated the presence of more than one magnetic species in the protein samples, however, with g values depending on pH, buffer, counterion, freezing rate, and the presence of glass-forming agents. Since a homogeneous sample was desirable for a quantitative analysis, we finally chose to study the benzohydroxamic acid complex of the enzyme. Schonbaum (1972) has shown that addition of benzohydroxamic acid, which binds to the protein rather than to the heme iron, yields a single, sharp EPR signal as illustrated in Figure 1. The signal arises from the lowest Kramers doublet of the $S = {}^5/_2$ spin sextet and has effective g values of 6.10, 5.46, and 1.98 (Colvin et al., 1983). The fact that the sum of g_x and g_y is less than 12 is not compatible with the second-order spin Hamiltonian, eq 1, which predicts $g_x \simeq 6 + 24(E/D)$ and $g_y \simeq 6 - 24(E/D)$ to first order in the rhombicity E/D if the spin-only value $g \simeq 2$ is substituted for $\mathbf{g}$ in the $S = {}^5/_2$ representation. Inclusion of fourth-order terms in eq 1 reduces the effective g_x and g_y insignificantly. As suggested by Maltempo & Moss (1976), the low g values of horseradish peroxidase imply an admixture of low-lying quartet states to the ground sextet via spin–orbit interaction. To account for this admixture within the spin-Hamiltonian model, we can use an anisotropic g tensor, $\mathbf{g} = (1.925, 1.925, 1.99)$ in the $S = {}^5/_2$ representation. The three-term model of Ristau (1980), which takes explicit account of the ${}^4T_1$ and ${}^2T_2$ excited states, reproduces the experimental g values and the zero field splitting with a 10.8% ${}^4T_1$ and 0.3% ${}^2T_2$ admixture to the ${}^6A_1$ ground state (see Discussion). Simulations of the EPR spectrum with the g-strain model described in the Appendix show that the observed spectral shape is best fitted by a nearly isotropic intrinsic Gaussian line shape of standard deviation $\sigma = 1.5$ mT. Adopting this value, any distribution in E/D, which must be centered at $E/D = 0.014$ to fit the data, cannot have a standard deviation $\sigma(E/D)$ in excess of 0.006.

The Mössbauer spectra of the benzohydroxamic acid complex of native horseradish peroxidase are shown in Figure 2. At temperatures of 4.2 K and below, we observe the six-line

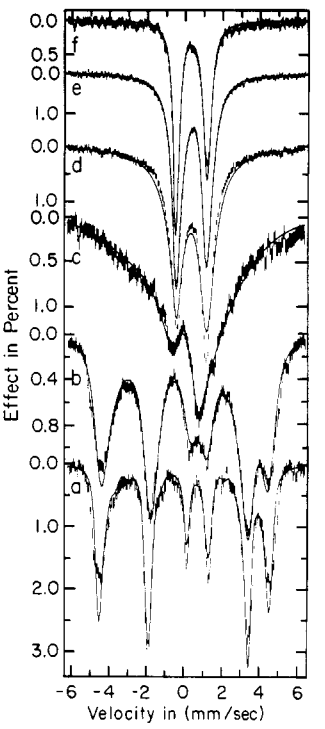

FIGURE 2: Mössbauer spectra of the benzohydroxamic acid complex of native enzyme at (a) 4.2, (b) 10, (c) 20, (d) 36, (e) 60, and (f) 200 K. A magnetic field of 0.17 T (34 mT at 60 and 200 K) was applied perpendicular to the direction of the γ beam. The solid lines are computer simulations based on eq 3, the spin-Hamiltonian $\hat{\mathcal{H}}_e = D'(\hat{S}_z^2 - 2/3) + E'(\hat{S}_x^2 - \hat{S}_y^2) + F'(7\hat{S}_z^4/36 - 95\hat{S}_z^2/72 + 63/64) + \beta_e \tilde{S}\cdot\mathbf{g}\cdot\vec{H}$, and the spin fluctuation model referred to in the text. The parameters are $\mathbf{g} = (1.925, 1.925, 1.99)$, $\mathbf{A}/(g_n\beta_n) = -(19.5, 17.5, 20)$ T, $D'/k = 30.2$ K, $E'/k = 0.26$ K, $F'/k = 12.3$ K, $\Delta E_Q = 1.59$ mm/s for $T \leq 60$ K and 1.64 mm/s for $T = 200$ K, $\eta = 0.25$, $\delta_{Fe} = 0.39$ mm/s for T ≤ 60K and 0.36 for T = 200 K, and $\Gamma = 0.3$ mm/s. The fluctuation model assumed a Debye temperature of 200 K, fractal dimension $d = 1.7$, and rate parameter $W_0 = 1.46 \times 10^5$ rad s^{-1} $K^{-1.7}$.

spectrum of Figure 2a in a field of 170 mT. This pattern is typical for high-spin ferric heme iron, although the peaks are rather broad and the overall splitting of ~9 mm/s is relatively small. Simulations based on eq 1 with the parameters listed in the figure caption reproduce the data quite well. We assumed the principal axes of the quadrupole and the fine-structure tensors to coincide; with this constraint, we could not find an adequate solution unless we let the hyperfine interaction $\mathbf{A}$ (in the spin $S = {}^5/_2$ representation) be slightly anisotropic.

At 12.5 K and higher temperatures, spin fluctuations cause the magnetic hyperfine interaction to gradually average out, and already at 60 K a relatively sharp quadrupole doublet emerges. All the spectra can be simulated by using a dynamic line-shape model (Schulz & Debrunner 1984), which accounts for arbitrary spin fluctuation rates. The spin transition rate is dominated by an Orbach process (Orbach & Stapleton, 1972) and therefore depends sensitively on $E_{ij}/(kT)$, where E_{ij} is the energy difference between Kramers doublets i and j. In fact, the model best fits the data with $(E_2 - E_1)/k \approx 40$ K and $(E_3 - E_1)/k \geq 170$ K, which gives us an estimate of the energies E_2 and E_3 of the second and third Kramers doublet. These estimates are not compatible with eq 1, which predicts $E_2 - E_1 \sim 2D$, $E_3 - E_1 \sim 6D \sim 3(E_2 - E_1)$ for $S = {}^5/_2$, and $E \ll D$. We will show under Discussion that the energies can be explained by the three-term model of Ristau (1981) or, phenomenologically, by the addition of a quartic term to eq 1. The fact that we can get successful simulations for all the data lends confidence to the parametrization used,

Table I: Parameters Deduced from Mössbauer Data of Ferryl Spin $S = 1$ Heme Compounds

	δ_{Fe}[a]	ΔE_Q[a]	D/k (K)	$A_\perp/(g_n\beta_n)$ (T)	$A_\parallel/(g_n\beta_n)$ (T)
HRP I	0.08	+1.25	37[b]	−19.3	−6
HRP II	0.03	+1.61	32	−19.3	−6.5
HRP X	0.07	1.51			
Mb(Fe^{IV})[c]	0.09	+1.43	35	−18.7	−2.5
CPO I[d]	0.15	+1.02	52	−20.2	−1
JRP I[e]	0.10	1.33			
JPP II[e]	0.11	1.46			
CCP-ES[f]	0.05	+1.55	28	−18.7	−6.5
TMP A[g]	0.06	+1.62	27	−22.1	−9.9
Fe(O)(TPP)(1-mIm)[h]	0.11	+1.26	33	−19.4	
Fe(O)(TPP)(pyr)[h]	0.10	+1.56	36	−19.6	

[a] Isomer shift δ_{Fe} and quadrupole splitting ΔE_Q in mm/s at 4.2 K except for JRP, 77 K. Typical uncertainty ±0.02 mm/s. [b] Colvin et al. (1983). [c] Schulz et al. (1979). Harami et al. (1977) measured compound II of Japanese radish peroxidase and the reaction product of myoglobin with H_2O_2 in strong fields at 4.2 K. The zero field splitting, $D/k = 18$ K, $E/D \leq 0.2$, and the magnetic hyperfine tensor $A/(g_n\beta_n) = -(3.28, 5.71, -0.86)$ T deduced by these authors are not compatible with high-field data taken over a larger range of temperatures (Schulz et al., 1979a) and are therefore not included in this table. [d] Compound I of chloroperoxidase (Rutter, 1982). [e] Compounds I and II of Japanese radish peroxidase at 77 K (Maeda & Morita, 1967). [f] Cytochrome *c* peroxidase compound ES (Lang et al., 1976). Values quoted for D and A are calculated by perturbation theory (Oosterhuis & Lang, 1973) from the parameters quoted by Lang et al. (1976). [g] Oxidized chloro-5,10,15,20-tetra(mesityl)porphyrinatoiron(III) (Boso et al., 1983). [h] Measurements of Simonneaux et al. (1982) on frozen toluene solutions. D and $A_\perp$ were estimated from the $\omega_\perp(T)$ values quoted in Table II of these authors by setting $\omega_\perp(T) = -A_\perp\langle S_x\rangle/(H\beta_n g_n)$, where $\langle S_x\rangle$ is the thermal average of the spin expectation value calculated from the Hamiltonian $\hat{\mathcal{H}}_e = D(\hat{S}_z^2 - 2/3) + \beta g_x \hat{S}_x H$, $g_x \simeq 2 + 4D/\zeta$ (Oosterhuis & Lang, 1973).

but further refinements in the model are possible.

Compound II. Compound II is 1 oxidizing equiv above native HRP and is thus in an EPR-silent, non-Kramers state. Theorell & Ehrenberg (1952) deduced an effective spin of $S = 1$ from susceptibility measurements at room temperature. Mössbauer measurements agree with this result and provide further details about the electronic state of the heme iron (Table I). From the isomer shift δ_{Fe}, which is a measure of the *s*-electron density at the iron nucleus, $\delta_{Fe} = 0.03$ mm/s at 4.2 K, the unusual charge state Fe^{4+} could be established (Moss et al., 1969). We have earlier deduced the spin-Hamiltonian parameters from high-field, variable-temperature Mössbauer measurements (Schulz et al., 1979a). In a field of $B = 4$ T and for $T \geq 26$ K, the data are compatible with the limit of fast spin fluctuation; assuming the standard Debye model, a lower limit of the fluctuation rate parameter W_0 can be established, which is $W_0 \geq 8.8 \times 10^3$ rad s^{-1} K^{-3}. Simulation of the spectra with eq 1 and 3 established that the heme iron is indeed in a spin $S = 1$ state with a large positive zero-field splitting $D \simeq 32 \pm 3$ K, that the quadrupole splitting $\Delta E_Q = 1.51 \pm 0.01$ mm/s is positive and independent of temperature up to 150 K, and that **g** and the magnetic hyperfine tensor A are as given in Table I. The data are compatible with axial symmetry of all the terms in eq 1 and 3; the simulations are insensitive to the rhombicity E/D, though, and finite E/D values can be accommodated with slight readjustment of the x and y components of the A tensor. All experimental results thus support a $(t_{2g})^4$, $S = 1$ configuration of the heme iron in compound II.

Compound I. Compound I, early recognized because of its unusual green color as the primary reaction product of HRP with peroxide, is 2 oxidizing equiv above the native, ferric state and like the latter has an odd number of unpaired spins. No

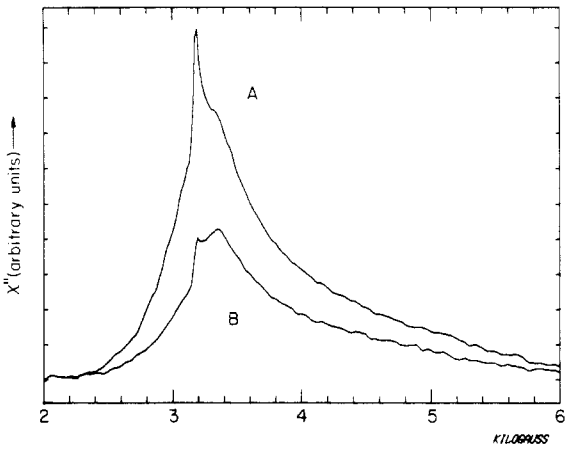

FIGURE 3: EPR absorption spectra of compound I recorded at 2.1 K with (A) 0.2- and (B) 20-μW microwave power at 8.883 GHz. The traces represent the absorption signals χ'' in arbitrary units observed at a sweep rate of 13.3 mT/s with no field modulation. We are indebted to Drs. G. Feher and R. Isaacson for recording these spectra.

EPR signal of the expected intensity had been found (Aasa et al., 1975) prior to 1979, however, when Schulz et al. (1979b) first observed a very broad, featureless EPR line centered at $g \simeq 1.99$. The signal was explained as resulting from a porphyrin cation radical, long postulated by Dolphin and others (Dolphin et al., 1971), which couples magnetically with the spin $S = 1$ ferryl center. Several recent studies, including the present one, substantiate this assignment (Roberts et al., 1981a,b). Figure 3 shows the EPR absorption spectrum recorded at 2.1 K by sweeping through the resonance at a rate of 13.3 mT/s with no field modulation. Again, a featureless, broad line at $g = 1.99$ is seen that slopes smoothly toward low and high fields. The narrow signal superimposed on the broad line at $g = 2$ is a contamination that saturates at low power levels and varies from sample to sample. Double integration of the usual derivative spectra taken under proper conditions reproducibly yields 1 ± 0.1 unpaired electron per heme (Rutter, 1982). Moreover, EPR and optical titrations show a 1:1 relation between the absorbance change and the fraction of spins in the broad signal. The shape of the EPR line and, presumably, also the spin relaxation rate are pH dependent (Rutter, 1982), but no systematic study of this effect has been made.

The Mössbauer spectra of compound I consist of a quadrupole doublet with an isomer shift $\delta_{Fe} = 0.08 \pm 0.01$ mm/s at 4.2 K, a splitting $\Delta E_Q = 1.25 \pm 0.01$ mm/s that is independent of temperature up to 140 K, the highest temperature studied, and a line width of $\Gamma_{FWHM} = 0.31 \pm 0.01$ mm/s for $T > 10$ K. At $T \lesssim 4.2$ K, the Mössbauer lines spontaneously broaden, and a weak applied field affects the line shape considerably (Figure 4). The magnetic broadening is a clear indication that we are dealing with a Kramers system in the slow-fluctuation limit. We can indeed model the Mössbauer spectra if we augment the spin-Hamiltonian eq 1 by eq 2 with an exchange tensor $|\mathbf{J}|/k \approx 3$ K. Two additional samples prepared with no glycerol at pH 4.5 (50 mM acetate) and 7.5 (50 mM potassium phosphate) showed the same quadrupole splitting and isomer shift, but the magnetic broadening at 4.2 K was larger in the pH 7.5 sample.

Mössbauer spectra observed at various temperatures with externally applied fields are shown in Figures 4 and 5. The high-field spectra, especially those taken at $T \geq 20$K, strongly resemble the corresponding spectra of HRP II with spin $S = 1$ and of related compounds (Schulz et al., 1979a; Lang et al., 1976; Harami et al., 1977). In spite of the fact that HRP I

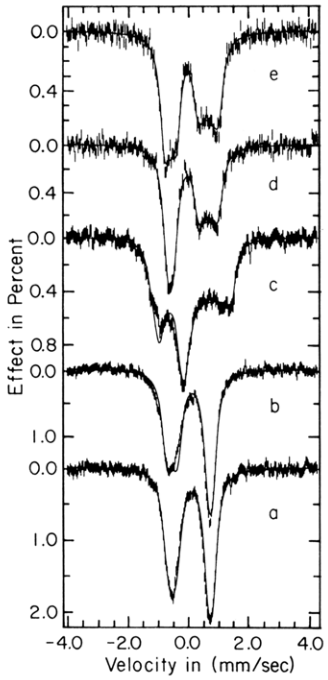

FIGURE 4: Mössbauer spectra of compound I measured under the following conditions: (a) 1.5 K, 44-mT perpendicular field; (b) 1.5 K, 44-mT parallel field; (c) 4.2 K, 5.5-T parallel field; (d) 26 K, 3.03-T parallel field; (e) 40 K, 3.03-T parallel field. The solid lines are simulations based on eq 1–3 with the parameters listed in Table I, a **g** tensor of (2.25, 2.25, 1.98) obtained by perturbation theory, an exchange term with $\mathbf{J}/k$ = (−4, −2, 6) K, and a spin fluctuation parameter $W_0 = 8.8 \times 10^4$ rad s^{-1} K^{-3}.

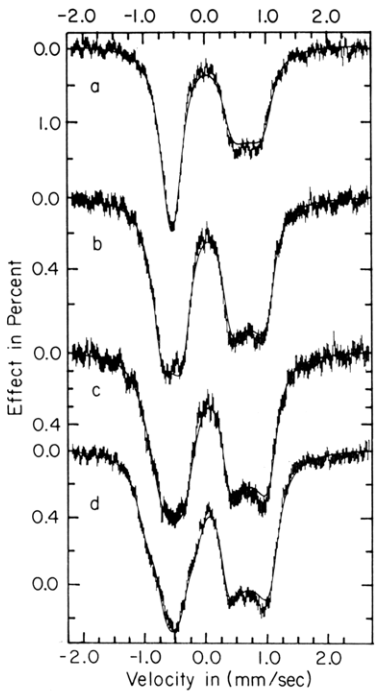

FIGURE 5: Mössbauer spectra of compound I at (a) 20, (b) 10, (c) 7, and (d) 4.2 K in an applied field at 2.5 T parallel to the γ beam. The solid lines are simulations based on the same model and parameter values as used in Figure 4.

is a Kramers system, one must apply strong fields in order to obtain substantial magnetic splittings at $T > 10$ K. The spin fluctuation rate is obviously fast under these conditions. For a given external field, the Mössbauer spectra vary with temperature, the broadening being smallest near 26 K. This minimum can be rationalized as due to a partial cancellation of the external field by an internal field; the temperature at

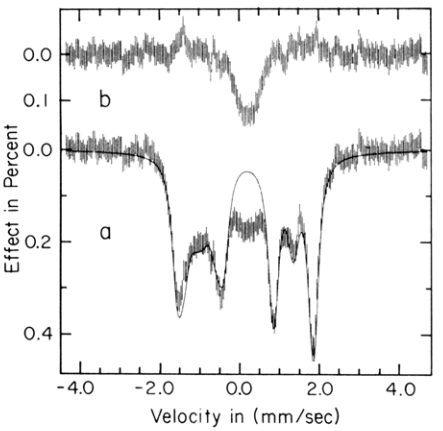

FIGURE 6: Mössbauer spectrum of compound III at 4.2 K in a field of 4.03 T parallel to the direction of the γ beam (a). The solid line is a spectrum simulated for a diamagnetic complex of quadrupole splitting $\Delta E_Q = -2.31$ mm/s, $\eta = 0$, and isomer shift $\delta_{Fe} = 0.24$ mm/s. Spectrum b is the difference between the experimental data and the simulation.

which it occurs allows an estimate of the zero field splitting D. From simulations such as those shown by solid lines in Figures 4 and 5, we deduce the best set of parameters given in Table I.

Compound X. The Compound X sample prepared according to Shahangian & Hager (1982) had the same optical spectrum as compound II and showed a similar, but not identical, Mössbauer spectrum. A single quadrupole doublet was observed from 4.2 to 200 K with a splitting and line width that increased very slightly with temperature: $\Delta E_Q = 1.51$ mm/s and $\Gamma = 0.246$ mm/s at 4.2 K, and $\Delta E_Q = 1.53$ mm/s and $\Gamma = 0.264$ mm/s at 200 K, respectively. The isomer shift, $\delta_{Fe} = 0.07$ mm/s at 4.2 K, and the quadrupole splitting are listed in Table I together with the parameters of other oxidized heme complexes. No high-field measurements have been performed that could establish the spin state and the zero field splitting of compound X, but a comparison of the tabulated values suggests the same assignment of the heme iron as for all other higher oxidation states listed, i.e., $(t_{2g})^4$, Fe(IV), $S = 1$.

Compound III. Compound III is a nonphysiological state of HRP that can be reached by two alternative pathways: (i) by addition of a large excess of H_2O_2 to compound II or (ii) by reaction of dithionite-reduced enzyme with O_2. The Mössbauer samples were prepared by the first method. At the millimolar concentrations needed for Mössbauer measurements, compound III is not stable, and all samples studied contained noticeable admixtures of other species. In the spectra shown in Figure 6, the admixture consists of a single broad peak centered at ~0.25 mm/s and is most likely due to a hemochromogen-like decay product caused by H_2O_2-induced denaturation of the protein. The major component in the Mössbauer spectrum is a quadrupole doublet with a splitting of $\Delta E_Q = -2.31$ mm/s and isomer shift $\delta_{Fe} = 0.23$ mm/s at 4.2 K. No magnetic interaction is evident in small applied fields as expected for an integer-spin system. The spectrum observed in high field is well reproduced by a simulation based on a diamagnetic, $S = 0$ ground state, as shown by the solid curve in Figure 6.

Discussion

As shown in the previous section, the EPR and Mössbauer spectra can be parametrized in terms of a spin-Hamiltonian model. We now consider the most plausible implications of the experimental parameters on the nature of the iron site in

Table II: Comparison of Spin-Hamiltonian and Mössbauer Parameters, Equations 1 and 3, of Native Horseradish Peroxidase with Those of Other High-Spin Ferric Heme Proteins

	g_{eff}	D/k (K)	E/D	δ_{Fe}[a]	ΔE_Q[a]	η	H_{sat}[b]
HRP	6.1, 5.46, 1.98[c]	20.5[d]	0.014	0.40	1.60	0.25	−48.6[e]
CCP[f]	6, 6, 2	21.6	0	0.40	1.27		−49
CAT[g]	6.5, 5.5, 2		0.021	0.27	1.14	0.115	−48.8
I⁻CPO[h]	7.5, 4.2, 1.8		0.07		0.65	0.1	−46
mMb[i]	5.98, 5.87, 2	14.4	0.003		0.65		−49.8
P-450$_{CAM}$[j]	8, 4, 1.8	5.5	0.087	0.44	0.78	0.6	−45
cyt c' I[k]	5.9, 5.7, 2	21.6	0.005	0.37	1.35	−0.2	−46.1
cyt c' II[l]	5.8, 5.6, 2	>29	0.005	0.37	1.65	−0.2	−43.7

[a] Isomer shift δ_{Fe} and quadrupole splitting ΔE_Q at 4.2 K in mm/s. Typical uncertainty ±0.02 mm/s. [b] Saturation field defined as $H_{sat} = (5/2)\langle A_i/g_i\rangle 2/(g_n\beta_n)$, i = 1, 2, and 3, in units of T. [c] Corresponds to $g_\perp = 1.93$ and $g_\parallel = 1.99$ in the $S = {}^5/_2$ representation. [d] Colvin et al. (1983). Note that eq 1 predicts the third Kramers doublet at too low an energy (see Discussion). [e] Note anisotropy, $A/(g_n\beta_n) = -(19.5, 17.5, 20)$ T, required in simulations of Figure 2. [f] Cytochrome c peroxidase (Lang et al., 1969). [g] Catalase (Parak et al., 1979). [h] Chloroperoxidase iodide (Champion et al., 1973). [i] Metmyoglobin (Slade & Farrow, 1972). [j] Substrate complex of cytochrome P-450$_{CAM}$ (Tsai et al., 1970; Sharrock et al., 1976). [k] Cytochrome c' form *Rhodospirillum rubrum*, pH 7, majority species (Emptage et al., 1977). [l] Minority species (40%) of above (footnote k).

the various enzymatic states. Since the structure of HRP is not known, much of the interpretation of our data rests on inferences based on comparisons with better known systems, in particular myoglobin, cytochrome c peroxidase (Poulos & Kraut, 1980), catalase (Murthy et al., 1982), and model compounds. On the basis of the known sequence and other data, Welinder (1979) suggests a model of two domains with the heme in between. All evidence implicates histidine as the proximal iron ligand (La Mar et al., 1982). The distal ligand, if any, obviously changes in the course of the reaction as will be discussed.

Native Horseradish Peroxidase. The EPR and Mössbauer spectra of the high-spin ferric, native enzyme reveal several salient features. (i) The magnetic properties of the heme iron are easily perturbed by pH, buffer, and substrates, which apparently bind in the second coordination sphere (Schonbaum, 1972; Burns et al., 1975). Multiple EPR species are quite common (Maltempo et al., 1979). (ii) The g tensors are rhombic with E/D ratios ~0.014, intermediate between those of metmyoglobin and catalase but considerably less rhombic than those of high-spin chloroperoxidase or cytochrome P-450 (see Table II and references cited therein). (iii) The average of $g_\perp$, $\langle g_\perp\rangle = 5.78$ for the benzohydroxamic acid complex, is considerably smaller than the value $\langle g_\perp\rangle \approx 6$ expected for a pure spin sextet. Binding of phenols or quinones lowers $\langle g_\perp\rangle$ even further (Maltempo et al., 1979). (iv) The zero field splitting $(E_2 - E_1)/k \approx 41$ K, first estimated from Mössbauer data (Schulz, 1979) and later confirmed by more accurate EPR saturation recovery measurements (Colvin et al., 1983), is one of the largest values reported for high-spin ferric heme proteins. (v) The quadrupole splitting, $\Delta E_Q = 1.6$ mm/s, is the largest one found in an $S = {}^5/_2$ heme. Moreover, the charge distribution at the iron has less than axial symmetry as indicated by the asymmetry parameter, $\eta = 0.25$. Catalase and high-spin chloroperoxidase show finite η values as well.

All these features are quite exceptional for a high-spin ferric heme with its $(3d)^5$, nominal $^6A_1$ ground state. They presumably arise from an unusual coordination of the proximal histidine and possibly of a distal water. In metmyoglobin, a water molecule is weakly coordinated to the heme iron, and H_2O or OH^- has been identified as a sixth ligand in crystalline cytochrome c peroxidase (Poulos & Kraut, 1980). The situation for HRP, on the other hand, is ambiguous. According to Gupta et al. (1979), protons exchange from a site near the iron, but this site is either not fully occupied or too far from the iron to arise from bound water. The presence or absence of a water ligand might well affect the EPR spectra, and since an ionizable group interacts with the heme (Kitagawa & Teraoka, 1982), the pH and buffer dependence of the EPR signals might be explained by this mechanism. An ENDOR search for water protons of different EPR species might give a definitive answer.

We next explore the question of whether an unusual histidine coordination can explain some of the anomalies listed above. Suppose that the bond between the histidine nitrogen and the heme iron has weaker σ character than that in metmyoglobin and cytochrome c peroxidase but has some π character instead. This may come about if the nitrogen sp^2 lone pair is not in line with the iron d_{z^2} orbital. As a consequence, the antibonding iron d_{z^2} orbital will be lowered in energy relative to $d_{x^2-y^2}$, and one of the d_π orbitals will be raised relative to the other and will be differently populated. The latter results would lead to rhombic terms in the electric field gradient at the iron and in the zero field splitting. Moreover, it would allow delocalization of porphyrin π^* via d_π to the empty π^* of the histidine nitrogen and thus raise the ν_4, porphyrin A_{1g} resonance Raman frequency as observed (Kitagawa & Teraoka, 1982). The lowering of the iron d_{z^2} orbital relative to $d_{x^2-y^2}$ is conducive to a low quartet spin state, $S = {}^3/_2$, which can be admixed to the sextet ground state by spin–orbit coupling as suggested by Maltempo & Moss (1976). A low, orbitally nondegenerate quartet state gives rise to a large zero field splitting in agreement with experiment. The positive quadrupole splitting must arise from covalency effects; it implies a larger excess of electron density in the heme plane than in any other high-spin ferric heme.

While the qualitative arguments presented here appear plausible, they clearly need further testing. A structural basis must be found for the basic assumption of a weak axial Fe–N bond with some π-bond admixture, for instance, a tilt of the histidine plane away from the heme normal. In the absence of crystallographic data, the relative orientation of the histidine may best be explored by NMR or ENDOR, and the relevant distances can be determined by EXAFS. Once the geometry is known, a molecular orbital calculation can be attempted.

The arguments relating the g values and the zero field splitting to an excited spin quartet can be formulated quantitatively in terms of a crystal field model and are thus independent of any assumptions about the axial ligation of the heme iron. Depending on the data to be rationalized, the problem can be approached at different levels. Most authors focus on the EPR properties of the lowest Kramers doublet and model the effective g tensor and the energy of the second doublet with a quartet admixture (Maltempo & Moss, 1976; Brill et al., 1978). As pointed out under Results, we have, in addition, an estimate of the energy of the third Kramers doublet, $(E_3 - E_1)/k \sim 170$ K, which was obtained by fitting the temperature dependence of the Mössbauer spectra to a

fluctuation model (Schulz & Debrunner, 1984). The empirical energies of the three Kramers doublets are thus not compatible with the quadratic spin-Hamiltonian, eq 1, which represents the quartet admixture in second-order perturbation theory. We therefore resort to an exact diagonalization of a crystal field model (Ristau, 1981) that assumes rhombic symmetry, includes the excited spin quartet, and, for generality, includes also the spin doublet. Before we describe Ristau's three-term model, we briefly discuss the spin-fluctuation model, which led to the crucial energy estimate of the third Kramers doublet.

It should be pointed out that the simulation of the data in Figure 2 is the first of its kind for a high-spin ferric heme, covering the whole range of fluctuation rates from the slow limit at 4.2 K to a fast rate at 200 K with a single set of parameters. The model correctly accounts for the changing asymmetry of the spectra with temperature, and it yields an energy of the second Kramers doublet (Schulz, 1979) in agreement with EPR saturation recovery (Colvin et al., 1983). In spite of the obvious success of the model as applied to this and other systems (Schulz & Debrunner, 1984), its general validity at higher temperatures remains to be demonstrated.

Given the eigenstates of the spin sextet, the model makes simplifying assumptions about the spin–lattice coupling and the phonon spectrum. Spin transitions due to direct, intradoublet processes and the interdoublet, Orbach processes are modeled with a single adjustable rate parameter W_0. Transition rates are calculated by using a Debye model in the long-wavelength limit, assuming a phonon density of states of dimensionality 1.7, which is typical for a globular protein (Allen et al., 1982). A second adjustable parameter can be introduced for Raman processes. Order of magnitude estimates indicate, however, that Raman processes are insignificant up to $T \sim 160$ K, and the model calculations confirm that they must be negligible in the present case. Within this model the quadratic spin Hamiltonian, eq 1, is inadequate to reproduce all the spectra, primarily because it predicts the third Kramers doublet at too low an energy, $(E_3 - E_1)/k \sim 6D/k \sim 120$ K, given the energy $(E_2 - E_1)/k \sim 2D/k \sim 40$ K of the second doublet. Good simulations are obtained, however, with a quartic spin Hamiltonian on the basis of Ristau's model, which reproduces the effective g values and places the higher doublets at 40 and 177 K above the ground doublet. An independent determination of the fine structure would be valuable, and magnetic susceptibility is a promising technique for this purpose. Schonbaum (1973) reported agreement with Curie's law between 80 and 250 K and an effective magnetic moment of $n_{\text{eff}} = 5.97$, exceeding the theoretical limit of $\sqrt{35} \simeq 5.92$ for a pure spin $S = {}^5/_2$. We question these results, which are contrary to our expectations, and would like to see the measurements extended to lower temperatures and higher fields.

The three-term model adopted (Ristau, 1981) includes the lowest term $(t_{2g})^3(e_g)^2$, $^6A_1$, and the two higher terms $(t_{2g})^4e_g$, $^4T_1$, and $(t_{2g})^5$, $^2T_2$. The 3-fold orbital degeneracy of the T terms is lifted by crystal field components of axial and rhombic symmetry, and the $^4T_1$ term splits into the states ^4A_z, ^4B_x, and ^4B_y. The spin–orbit interaction $\zeta\vec{l}\cdot\vec{S}$ mixes the quartet and, to a lesser degree, the doublet with the ground term $^6A_1$, giving rise to the splitting of the sextet into three Kramers doublets. The stronger the admixture of excited states, the lower the effective g values of the ground state will be.

The three-term model depends on the Racah parameters B and C of the $(3d)^5$ configuration, taken to be $B = 1010$ cm^{-1} and $C = 4800$ cm^{-1} (Kotani, 1968), the cubic crystal field splitting $10Dq$, two axial splittings ρ and μ, the rhombic splitting R, and the spin–orbit coupling ζ. The latter was taken to be 350 cm^{-1}, i.e., substantially lower than the free ion value of 435 cm^{-1}. This reduction is consistent with a ligand field model, which allows mixing of the 3d orbitals with ligand orbitals of appropriate symmetry. The crystal field parameters are adjusted to best reproduce the experimental data, specifically (i) the effective g values (6.10, 5.46, 1.98) of the ground Kramers doublet, (ii) the energy $(E_2 - E_1)/k = 41$ K between the lowest two doublets (Colvin et al., 1983), and (iii) the energy $(E_3 - E_1)/k \sim 170$ K required to fit the high-temperature Mössbauer data. These constraints are not sufficient to determine the four crystal field parameters $10Dq$, ρ, μ, and R uniquely, however. We therefore eliminated one of the axial parameters by imposing the condition $\rho = 1.2\mu$ to find a solution with the following (nonunique) set of parameters: $10Dq = 29828$ cm^{-1}, $\rho = 7686$ cm^{-1}, $R = 369$ cm^{-1}. The quartet admixture (|amplitude|^2) to the low-lying sextet is found to be 10.8% while the doublet admixture is only 0.3%.

Given the exact eigenstates of the three-term model, we can calculate an effective spin Hamiltonian for the ground sextet. In general, one must add fourth-order terms of cubic, axial, and rhombic symmetry to eq 1 (Abragam & Bleaney, 1970). We find, however, that only the fourth-order axial term $F'(7\hat{S}_z^4/36 - 95\hat{S}_z^2/72 + 63/64)$ is significant in the case of horseradish peroxidase. The parameters of the effective Hamiltonian then are $D'/k = 30.2$ K, $E'/k = 0.26$ K, $F'/k = 12.3$ K, and $\mathbf{g}' = (1.925, 1.925, 1.99)$. The simulation of the Mössbauer spectra in Figure 2 is based on these parameters.

The three-term model thus adequately describes the fine structure of the $^6A_1$ multiplet and its EPR spectra. The given experimental data do not specify the model uniquely, and more could be learned from its application to other ferric hemes with substantial quartet admixture. A potential test of its validity would be the prediction of the electric and magnetic hyperfine interactions as observed in the Mössbauer spectra. Indeed, the three-term model justifies the use of an anisotropic hyperfine interaction in the simulations of Figure 2. We made no attempt to calculate the quadrupole interaction in view of the fact that the covalency contribution typically outweighs the valence contribution predicted by crystal field models for high-spin ferric iron.

The Spin $S = 1$, Ferryl State of Compounds I and II. We showed earlier that all Mössbauer data of compound II are compatible with the assignment of a spin $S = 1$ Fe(IV) state to the heme iron (Schulz et al., 1979a), and we pointed out that the same assignment with very similar parameters applies to compound I as well (Schulz et al., 1979b). We based our conclusions on measurements in high fields from 4.2 to 90 K, which were simulated by using the phenomenological spin Hamiltonian, eq 1 and 3, with adjustable parameters D, E, η, and $\mathbf{A}$. Several Mössbauer studies of heme compounds in higher oxidation states can now be compared, and a representative sample of the results is listed in Table I. To the extent that the magnetic properties of the iron in these compounds have been determined, they are all compatible with a ferryl state of spin $S = 1$. Compound ES of cytochrome c peroxidase was the first of these systems to be analyzed in strong external fields as a function of temperature (Lang et al., 1976). The spectra were successfully simulated in terms of a crystal field model based on a spin $S = 1$ $(t_{2g})^4$ configuration (Oosterhuis & Lang, 1973). The model introduces, in addition to the dominant octahedral crystal field, components of axial and rhombic symmetry and the spin–orbit interaction, which lift the degeneracy of the t_{2g} orbitals. If the problem

is restricted to axial symmetry, the only adjustable parameter of the model is the axial crystal field Δ.

While the assumptions of this model differ from ours, which are expressed in eq 1 and 3, it is possible to approximate the crystal field model by a spin Hamiltonian for all Δ values of interest. Conversely, most of the spin-Hamiltonian parameters of compounds I and II are reasonably well reproduced by the model of Oosterhuis & Lang (1973). From the zero field splitting $D/k \simeq 32$ K, we find an axial crystal field $\Delta/\zeta \approx 5.4$ in units of the spin–orbit coupling constant ζ, and the model then predicts $\Delta E_Q \sim 2.9$ mm/s and $\mathbf{A}/\beta_n g_n = -(17.3, 17.3, 6.7)$ T. Whereas the latter is close to the experimental value, the model overestimates the quadrupole splitting by roughly a factor of 2. This discrepancy, which is common to all compounds in Table I, arises from the fact that the crystal field model accounts for the electric field gradient due to the $(t_{2g})^4$ valence electrons only, while other configurations and the equally important covalency contributions are ignored. A molecular orbital calculation by Loew & Herman (1980) predicts $\Delta E_Q = 1.43$ mm/s in fair agreement with the data.

The Mössbauer parameters in Table I appear strikingly similar, especially if they are contrasted with the values typical of other oxidation and spin states of the heme iron (Lang, 1970). The similarity holds equally well for compounds that are 1 or 2 oxidation equiv above the ferric state; it strongly suggests a common electronic state of the heme iron in all compounds listed and most likely also a common axial ligand. This state is readily parameterized in terms of a spin $S = 1$ Hamiltonian, eq 1 and 3, and the small isomer shift, $0.03 \text{ mm/s} \leq \delta_{Fe} \leq 0.15$ mm/s, indicates a formal charge state of Fe(IV). Further characteristics are the large positive zero field splitting, $27 \text{ K} \leq D/k \leq 52$ K, the positive, axial quadrupole splitting, $1.01 \text{ mm/s} \leq \Delta E_Q \leq 1.61$ mm/s, and an axial magnetic hyperfine tensor A. Another proof of the essential similarity in the electronic structure comes from the fact that all experimental data are compatible with a common symmetry axis[1] of the zero field splitting, the electric field gradient, and the magnetic hyperfine tensor. According to the crystal field model, the heme normal must be this common axis of symmetry.

In all likelihood, the heme iron in all compounds of Table I is coordinated to a single oxygen atom, and it is in fact the oxo coordination that conveys the specific characteristics to the heme iron. The ferryl nature is obvious for the model complexes Fe(O)(TPP)(1-MeIm) and Fe(O)(TPP)(Py) (Simonneaux et al., 1982) and compound A of FeTMP (Boso et al., 1983); it has been proven by isotope experiments for compounds I of chloroperoxidase (Hager et al., 1972) and horseradish peroxidase (Roberts et al., 1981b), and it is consistent with chemical evidence for compounds I and II. Recent EXAFS data indicate an iron–oxygen distance of 1.6 Å in these ferryl complexes (Penner-Hahn et al., 1983). It is interesting to note that no clear-cut influence of the other axial ligand of the heme iron is discernible; this ligand is a nitrogen base in all cases except for chloroperoxidase and compound A.

Turning now to the variations in isomer shift, δ_{Fe}, quadrupole splitting, ΔE_Q, and zero field splitting, D, among the spin $S = 1$ ferryl states, we find empirically that the protein data can be approximated by the linear relations

$$\delta_{Fe} = -0.090 + 0.00463D/k$$

and

$$\Delta E_Q = 2.27 - 0.0245D/k$$

where δ_{Fe} and ΔE_Q are given in mm/s and D/k is given in K. These linear relations reproduce the data better than the assumption of constant δ_{Fe} and ΔE_Q, but as more and better measurements become available, the coefficients may change, and more complex relationships may emerge.[2] The two equations also imply the linear dependence $\delta_{Fe} = 0.33 - 0.18\Delta E_Q$, with a correlation coefficient $R = -0.94$.

The correlations between quadrupole splitting, isomer shift, and zero field splitting expressed by the equations above cannot be explained in the framework of the $(t_{2g})^4$ crystal field model of Oosterhuis & Lang (1973); they call for a molecular orbital calculation or a ligand field approach that allows for different delocalization of different iron orbitals. Increasing δ_{Fe} implies lower s-electron density at the iron, which is typically the result of increased shielding by the 3d or 4p electrons. The small magnitude of the observed change in δ_{Fe} is compatible with an indirect, shielding effect. A decrease in the (positive) quadrupole splitting means removal of the excess negative charge in the heme plane or addition of charge along the heme normal. An increase in the population of the d_π or $4p_z$ orbitals with increasing zero field splitting could account for the observed effect.

Compound I. Of all reaction intermediates in the enzymatic cycle of horseradish peroxidase the primary compound is the most intriguing. Although unambiguously identified by optical, Mössbauer, EPR, NMR, and ENDOR spectroscopy as a spin-coupled oxoferryl porphyrin π-cation complex with a histidine coordinated to the iron, neither the exact geometry of the complex nor the details of its wavefunction are known. The Mössbauer parameters of compound I strongly resemble those of compound II and all other compounds in higher oxidation states (Table I), leaving no doubt that the electronic configuration of the heme iron is basically the same in these complexes. The isomer shift, in particular, $\delta_{Fe} = 0.08$ mm/s, is a unique signature of the ferryl state. The Mössbauer spectra recorded in applied fields for $T > 10$ K can be adequately parameterized by a spin $S = 1$ Hamiltonian, eq 1 and 3, with a large, positive zero field splitting $D/k \sim 35$ K. All data are compatible with axial symmetry ($E = 0$, $\eta = 0$, $g_x = g_y \neq g_z$, $A_x = A_y \neq A_z$) although small rhombic terms cannot be excluded. The spontaneous magnetic hyperfine broadening observed in low-temperature, low-field Mössbauer spectra was the first evidence that the $S = 1$ ferryl iron in compound I is spin coupled to a Kramers system of spin $S' = {}^1/_2$. We assume that the coupling between the spins S and S' can be modeled by an exchange interaction $\hat{\mathcal{H}}_e' = \vec{S}\cdot\mathbf{J}\cdot\vec{S}'$, eq 2, where J is a phenomenological 3×3 matrix. The primary compound, which is 2 charge units above the native, ferric state, evidently has an odd number of electrons and is therefore expected to be EPR active. On the basis of optical comparisons with oxidized Zn(II) and Cu(I) porphyrins, Dolphin et al. (1971) suggested that the spectrum of compound I is indicative of a porphyrin π-cation radical, which again should be EPR active. However, prior to 1979, all efforts to observe the EPR signal of compound I revealed only minute fractions of an unpaired electron (Aasa et al., 1975) for reasons

[1] It is difficult to differentiate experimentally between axial and rhombic symmetry. The only positive indication of rhombic distortion is found in compound I of chloroperoxidase, whose EPR spectrum has been reproduced with $E/D \sim 0.035$.

[2] The correlation coefficients are $R = |m\sigma_x/\sigma_y| \approx 0.92$. If the three model compounds in Table I are included, the relations are $\delta_{Fe} = -0.055 + 0.0040D/k$ and $\Delta E_Q = 2.23 - 0.023D/k$ with correlation coefficients $|R| \simeq 0.82$.

that are now obvious. Due to spin coupling of the $S' = {}^1/_2$ porphyrin radical with the $S = 1$ ferryl iron, the EPR resonance is extremely broad and T_1 is much shorter than is typical for a radical. The broadness of the resonance makes the absorption derivative $d\chi''/dH$ very small, and great care has to be taken to differentiate between the signal and a nonideal base line. The longitudinal relaxation time T_1 is strongly temperature dependent, and values that provide good signal-to-noise ratios are obtained at $T < 10$ K only. In our original study we used the dispersion-derivative rapid-passage conditions[3] to record an absorption-type EPR spectrum, and we showed that it agrees with the integral of a standard absorption derivative. Figure 3 is an absorption signal recorded without field modulation under rapid adiabatic passage conditions and represents the true, inhomogeneous line shape (Weger, 1960). Many EPR samples of compound I have been quantified with the result that from 90 to 105% of the expected spins are accounted for. A simultaneous optical and EPR titration showed that the characteristic optical spectrum of compound I correlates with the broad EPR spectrum (Rutter, 1982).

Since the ferryl iron has a large, positive zero field splitting $D/k \sim 35$ K, only the lowest Kramers doublet of the spin-coupled system is populated at the temperatures at which EPR is detectable. If the porphyrin radical is taken to have an isotropic g value, $g' \approx 2$, and if E/D is small, the effective g tensor of the ground doublet has a z component that differs from 2 only to second order in J/D, while the x and y components differ to first order in J/D, i.e., are larger or smaller than 2 depending on whether J is negative or positive. According to the crystal field model, the z direction represents the heme normal, but the x and y axes in the heme plane are not predetermined. It follows that the center of the EPR spectrum near $g = 2$ corresponds to g_z^{eff}, while the broad wings arise from the in-plane components g_x^{eff} and g_y^{eff}. The exchange interaction furthermore must have antiferromagnetic ($J > 0$, $g^{\text{eff}} < 2$) as well as ferromagnetic components ($J < 0$, $g^{\text{eff}} > 2$), both of approximate magnitude $|J| \sim D/10$. This situation can be modeled either by assuming a distribution in J that includes positive values as well as negative ones, by assuming a strongly anisotropic interaction of the dipole–dipole (tr $\mathbf{J} = 0$) type,[4] or by a combination thereof. A distribution of J values implies that different molecules have different exchange interactions, presumably as a result of slightly different heme ligand conformations analogous to the more familiar g strain. Highly anisotropic exchange, on the other hand, would appear to be quite unusual as in most coupled systems an isotropic J was found to explain all observations. On the basis of the EPR and Mössbauer spectra presented here, however, we cannot rule out anisotropy.

The relatively small exchange interaction, $|J/k| \sim 3$ K, may appear surprising at first sight in view of the close proximity of the paramagnetic centers and the known covalency of the heme group. To the extent that the unpaired porphyrin electron has a_{2u} symmetry as suggested by Dolphin et al. (1971), it has no overlap with the unpaired 3d electrons of the iron. The exchange interaction, which depends on the mixing of wave functions, should therefore be sensitive to (i) the energy of the iron $4p_z$ orbital, which has a_{2u} symmetry and is strongly affected by the axial ligands, and (ii) any admixture of t_{2g} character to the radical wave function. It is not unreasonable to assume that these factors vary with the local conformation of the heme environment and that J may differ from molecule to molecule. We should point out also that because $|J|$ is much smaller than D, $|J|/D \sim 0.1$, the total spin of the complex is not a good quantum number although the spin expectation value is of course measurable. The model predicts an effective magnetic moment of $n_{\text{eff}}/\beta = 2[S(S+1) + S'(S'+1)]^{1/2} = 3.32$ at room temperature in fair agreement with early susceptibility measurements, $n_{\text{eff}}/\beta = 3.92$ (Theorell & Ehrenberg, 1952).

It is instructive to compare horseradish compound I with other heme compounds of the same formal charge state, i.e., 2 oxidizing equiv above the ferric state.

(i) Compound ES of cytochrome c peroxidase was the first of these systems to be analyzed. It differs from compound I in that one of the oxidizing equivalents resides in a free radical on an amino acid residue rather than on the porphyrin, while the other equivalent is found on the spin $S = 1$, ferryl iron as in compound I. This difference in the reaction with peroxide is unexpected for the two proteins in view of the similarity of their active centers. Both contain high-spin ferric protoporphyrin IX with an axial histidine ligand in their native state. The quartet admixture and rhombicity that distinguishes the electronic state of native horseradish peroxidase from that of cytochrome c peroxidase can hardly account for the difference in their primary compounds. The reason is more likely a peculiarity of the protein part of cytochrome c peroxidase, which allows reversible formation of a radical with a redox potential intermediate between the Fe(III)/Fe(IV) couple and the Fe(IV) porphyrin radical. On the basis of EPR and ENDOR data, Hoffman et al. (1981) suggest a methionyl radical at a distance of at least 5.6 Å from the heme. In spite of this large distance, electron transfer between the porphyrin and the radical appears to proceed quite efficiently. We are led to this conclusion from the plausible assumption that the heme group is the site of the primary redox reaction with peroxide and the fact that no trace of a porphyrin radical, Fe(V), or similar intermediate is detectable.

(ii) Compound I of chloroperoxidase exhibits the same type of spin-coupled oxoferryl porphyrin radical complex as horseradish peroxidase in spite of the fact that the heme iron in native chloroperoxidase is coordinated to a cysteine sulfur in contrast to horseradish peroxidase with Fe–histidine coordination. Apart from the different reactivities of the two peroxidases, the major distinctions of chloroperoxidase compound I are its optical spectrum, which is of the catalase compound I type (Palcic et al., 1980), the larger zero field splitting, $D/k \sim 52$ K, of the spin $S = 1$ ferryl state, and a much larger exchange interaction, $J/k \sim 53$ K, between the spin $S = 1$ of the iron and the porphyrin radical. The last point leads to an EPR spectrum with g values $g_{\parallel} = 2.0$ and $g_{\perp} \approx 1.73$ and a Mössbauer spectrum with well-resolved magnetic hyperfine splittings at 4.2 K. With appropriate parameters, the spin-coupling model, eq 2, accounts for both primary compounds. The reason for the stronger antiferromagnetic exchange interaction in chloroperoxidase compound I is not known. It may be related to the stronger admixture of the iron $4p_z$ orbital in the axial bond, coupled with the fact that the unpaired electron of the porphyrin radical has some a_{2u} character in spite of Dolphin's prediction of a_{1u} character for catalase compound I type spectra.

[3] With $T_1 \sim 24$ ms $\gg T_2 \sim 1$ μs (Colvin et al., 1983), the experimental conditions correspond to case 7 of Weger (1960) rather than case 3 as originally stated (Schulz et al., 1979b).

[4] The through-space dipole–dipole interaction of the ferryl iron with the porphyrin radical is too small to account for the observed J values, contrary to our earlier suggestion (Schulz et al., 1979b). The exchange interaction therefore must arise from the overlap of the wave functions of the two paramagnetic centers.

Table III: Mössbauer Parameters of Compounds III and Other Oxygenated Heme Proteins as a Function of Temperature T (K)[a]

HRP III			JRP III[b]			MbO_2[c]			P-450–O_2[d]		
T	δ_{Fe}	ΔE_Q	T	δ_{Fe}	ΔE_Q	T	δ_{Fe}	ΔE_Q	T	δ_{Fe}	ΔE_Q
4.2	0.23	−2.31	77	0.29	(−)2.37	4.2	0.27	−2.31	4.2	0.31	−2.15
55	0.23	−2.30	195	0.24	(−)2.33	80	0.27	−2.23	82	0.29	−2.12
120	0.22	−2.30				193	0.23	−2.00	200	0.27	−2.07

[a] Isomer shifts δ_{Fe} and quadrupole splittings ΔE_Q in mm/s. Typical uncertainty ±0.02 mm/s. [b] Japanese radish peroxidase (Maeda & Morita, 1967). The sign of ΔE_Q is assumed to be negative in analogy to the other oxy adducts. [c] Oxymyoglobin. [d] Oxycytochrome P-450_{CAM} (Sharrock et al., 1975).

(iii) Groves and co-workers recently studied compound **A** of chlorotetra(mesityl)porphinatoiron as a model of compound I (Groves et al., 1981). The iron is indeed in the (oxo) ferryl state as shown by Mössbauer measurements (Boso et al., 1983), and the optical spectrum is indicative of a porphyrin radical. Interestingly, however, the exchange interaction is strong and ferromagnetic, leading to an effective spin of $S^{eff} = {}^3/_2$ at all temperatures. Compound **A** has a short iron–oxygen bond of 1.6 Å and, presumably, no further axial iron ligand (Penner-Hahn et al., 1983), but details of the geometry are not known, and the strong ferromagnetic coupling has not been rationalized yet.

This survey shows that a stable ferryl–porphyrin radical state is well established for heme proteins and model compounds. The optical spectra of the porphyrin radicals may differ, but the parameters of the heme iron are quite similar and are essentially those of compounds II.

The more subtle question of the exchange interaction between the two spins has not been treated properly yet. The parametrization of the EPR and Mössbauer spectra is not unique and needs to be refined with the help of ENDOR or spin-echo and susceptibility measurements. Judging from the variation in magnitude and sign of J observed for primary compounds of horseradish and chloroperoxidase and compound **A** of TMP, the exchange interaction appears to depend on structural details of the oxoferryl and the porphyrin radical that we cannot identify yet. Physiologically, the exchange coupling per se is hardly relevant, but its very existence provides a probe for those unknown structural details.

Compound X. Compound X is able to insert a chlorine atom into a suitable acceptor molecule, and it has been suggested that chlorine oxide is the axial ligand of the Fe(IV) heme in this enzymatic intermediate (Shahangian & Hager, 1982). The similarity of the isomer shift and quadrupole splitting of compound X and all other ferryl hemes listed in Table I leaves little doubt about the charge and spin state of the heme iron, which must be Fe(IV), $S = 1$, and an axially coordinated oxygen is likely. The lack of any magnetic hyperfine broadening in the Mössbauer spectra suggests that compound X is an integer spin system like compound II and is thus 1 oxidation equiv above the native, ferric state. The near identity of the optical spectra of compound X and compound II, which has been noted before, is compatible with this finding (Shahangian & Hager, 1982). There is a small, but well-established difference in the Mössbauer parameters of compounds II and X, which is compatible with, but no proof of, chlorine coordination to the ferryl oxygen.

Compound III. All evidence indicates that compound III is an oxygenated heme complex akin to oxymyoglobin and related O_2 adducts. The spectrum measured in high field, Figure 6, is best simulated by assuming a diamagnetic state of the iron and a negative, axially symmetric quadrupole interaction. As in oxymyoglobin, the quadrupole splitting decreases with increasing temperature, albeit at a smaller rate. The analogy of the heme complex in compound III and in other O_2 adducts is brought out in Table III, which lists the quadrupole splittings and isomer shifts as a function of temperature in comparison with oxymyoglobin and oxycytochrome P-450_{CAM}.

It should be pointed out that the O_2 adducts are the only known nominally low-spin ferrous heme complexes with such an unusually large and temperature-dependent quadrupole splitting. The electronic structure of the iron is apparently determined by the Fe–O_2 bond, the fifth, axial ligand provided by the protein playing only a minor role. Thus, while the Mössbauer data characterize the state of the heme iron in detail, they indicate that it is essentially the same as found in other O_2 adducts.

Conclusions

A detailed study of the electronic state of the heme iron in horseradish peroxidase reveals many unique features in the native enzyme, and it provides a basis of comparison for the higher oxidation states of compound I and II. We show that the Mössbauer and EPR data taken under a variety of conditions can be modeled consistently in a spin-Hamiltonian formalism, and the meaning of the derived parameters has been further illuminated by crystal field models.

In the native enzyme, the iron is in the high-spin ferric state but has substantial admixtures from the higher quartet states. The quartet admixture manifests itself in a large zero field splitting with an unusually high energy of the third Kramers doublet, $E_3/k \sim 170$ K, relative to the second doublet at $E_2/k \sim 41$ K, and in low and anisotropic g values of the sextet, $g_\perp = 1.925$ and $g_\parallel = 1.99$. In contrast to other high-spin ferric heme proteins with histidine axial ligands, the local symmetry at the iron is rhombic in horseradish peroxidase rather than axial, which may arise from some π admixture in the Fe–N_{His} bond.

In the primary and secondary compounds, the iron has the same oxidation state Fe(IV), and the $(t_{2g})^4$ configuration gives rise to a spin triplet, $S = 1$, with a large positive zero field splitting, $D/k \sim 35$ K. The parameters of the iron are very similar in both states, and it is suggested that the oxo ligand has a dominating influence on the electronic state of the iron. Comparison with other ferryl heme compounds supports this suggestion; it furthermore reveals a correlation between zero field splittings, quadrupole splittings, and, less firmly, isomer shifts.

In compound I the porphyrin is oxidized to a spin $S' = {}^1/_2$ π-cation radical, which couples weakly to the ferryl spin $S = 1$. The spin coupling can be modeled by a phenomenological exchange interaction $\vec{S}\cdot\mathbf{J}\cdot\vec{S}'$ with $|J| \sim D/10$, which accounts for the peculiarly broad EPR spectrum and the fast, strongly temperature-dependent spin relaxation of compound I. Other ferryl porphyrin radical complexes are described by the same model, but the large variation in magnitude and sign of the exchange parameter J required to fit the data has not been rationalized yet. Compound III, finally, has all the features familiar from other O_2 adducts of ferrous heme proteins, indicating that the Fe–O_2 bond determines the electronic state of this low-spin complex.

Appendix

Simulation of EPR Spectra with g-Strain Model. In order to interpret the inhomogeneous EPR spectra of native HRP, Figure 1, and compound I, Figure 3, a computer-simulation program was developed. The program performs a numerical "powder" integration over the angle Ω of the magnetic field $\vec{H}$ with respect to the principal axes of the spin system (Schulz, 1979) and uses an angle-dependent Gaussian line width deduced from the simple g-strain model described below. An adjustable lower limit of the width serves to simulate the intrinsic line width. A large zero field splitting is assumed, and transitions between different Kramers doublets are ignored.

The g-strain model adopted is based on the assumption that the major contribution to the line width arises from a distribution of some parameter λ in the spin-Hamiltonian eq 1 and 2. For a given λ, H, and Ω, the "spectrum" of a spin packet is approximated by a δ function:

$$S(\lambda, H, \Omega) = I_{\lambda\Omega}\delta(H - H_r) \quad (1A)$$

where $I_{\lambda\Omega}$ is the transition probability and H_r is the resonance field; $H_r = h\nu/(g\beta)$. If λ is varied by some small amount ϵ, we have

$$S(\lambda + \epsilon, H, \Omega) \approx (I_{\lambda\Omega} + \alpha\epsilon)\delta(H - (H_r + \gamma\epsilon)) \quad (2A)$$

where $\alpha \propto (\partial I/\partial\lambda)_{\lambda\Omega}$ and $\gamma \propto (\partial H_r/\partial\lambda)_{\lambda\Omega}$. If we integrate eq 2A over a Gaussian distribution in ϵ of width σ, we get

$$S(\lambda, H, \Omega) = \int_{-\infty}^{\infty} S(\lambda + \epsilon, H, \Omega) \exp[-(1/2)\epsilon^2\sigma^2] \times (2\pi\sigma^2)^{-1/2}\, d\epsilon = [I_{\lambda\Omega} + (H - H_r)\alpha/\gamma] \exp[-(1/2)(H - H_r)^2/(\gamma\sigma)^2](2\pi\gamma^2\sigma^2)^{-1/2}$$

The dispersion-type term $(H - H_r)\alpha/\gamma$ is typically small and can be neglected; thus, the model yields an angle-dependent Gaussian line width

$$W_{\lambda\Omega} = \sigma\gamma = \sigma(\partial H_r/\partial\lambda)_{\lambda\Omega} \quad (3A)$$

provided that

$$H_r/\sigma \gg (\partial H_r/\partial\lambda)_{\lambda\Omega} \quad (4A)$$

The relevant parameters that were distributed are the rhombicity E/D in the case of native, high-spin ferric HRP and the exchange tensor $\mathbf{J}$ in the case of compound I, respectively. The large width σ required for the latter violates the condition 4A; therefore, the distribution was approximated by an appropriately normalized sum of Gaussians of smaller width $\sigma' < \sigma$ such that eq 4A was satisfied for all angles Ω. For the benzohydroxamic acid complex of native HRP, Figure 1, an angle-independent line width gave the best results.

Registry No. Peroxidase, 9003-99-0; hydrogen peroxide, 7722-84-1; sodium chlorite, 7758-19-2.

References

Aasa, R., Vänngård, T., & Dunford, H. B. (1975) *Biochim. Biophys. Acta 391*, 259–264.

Abragam, A., & Bleaney, B. (1970) *Electron Paramagnetic Resonance of Transition Ions*, Clarendon Press, Oxford.

Adler, A. D., Longo, F. R., Kaupas, F., & Kim, T. (1970) *J. Inorg. Nucl. Chem. 32*, 2443–2445.

Allen, J. P., Colvin, J. T., Stinson, D. G., Flynn, C. P., & Stapleton, H. J. (1982) *Biophys. J. 38*, 299–310.

Boso, B., Lang, G., McMurray, T. J., & Groves, J. T. (1983) *J. Chem. Phys. 79*, 1122–1126.

Brill, A. S., Fiamingo, F. G., & Hampton, D. A. (1978) in *Frontiers of Biological Energetics* (Scarpa, A., et al., Eds.) Vol. 2, pp 1025–1033, Academic Press, New York.

Burns, P. S., Williams, R. J. P., & Wright, P. E. (1975) *J. Chem. Soc., Chem. Commun.*, 795–796.

Champion, P. M., Münck, E., Debrunner, P. G., Hollenberg, P. F., & Hager, L. P. (1973) *Biochemistry 12*, 426–435.

Chiang, R., Rand-Meir, T., Makino, R., & Hager, L. P. (1976) *J. Biol. Chem. 251*, 6340–6346.

Clauser, M. J., & Blume, M. (1971) *Phys. Rev. B: Condens. Matter 3*, 583–591.

Colvin, J. T., Rutter, R., Stapleton, H. J., & Hager, L. P. (1983) *Biophys. J. 41*, 105–108.

Cotton, M. L., & Dunford, H. B. (1973) *Can. J. Chem. 51*, 582–587.

Dolphin, D., Forman, A., Borg, D. C., Fajer, J., & Felton, R. H. (1971) *Proc. Natl. Acad. Sci. U.S.A. 68*, 614–618.

Emptage, M. H., Zimmerman, R., Que, L., Jr., Münck, E., Hamilton, W. D., & Orme-Johnson, W. H. (1977) *Biochim. Biophys. Acta 495*, 12–23.

Groves, J. T., Haushalter, R. C., Nakamura, M., Nemo, T. E., & Evans, B. J. (1981) *J. Am. Chem. Soc. 103*, 2884–2886.

Gupta, R. K., Mildvan, A. S., & Schonbaum, G. R. (1979) in *Biochemical and Clinical Aspects of Oxygen* (Caughey, W. S., Ed.) pp 177–193, Academic Press, New York.

Hager, L. P., Doubek, D. L., Silverstein, R. M., Hargis, J. H., & Martin, J. C. (1972) *J. Am. Chem. Soc. 94*, 4364–4366.

Harami, T., Maeda, Y., Morita, Y., Trautwein, A., & Gonser, U. (1977) *J. Chem. Phys. 67*, 1164–1169.

Hoffman, B. M., Roberts, J. E., Kang, C. H., & Margoliash, E. (1981) *J. Biol. Chem. 256*, 6556–6564.

Keilin, D., & Mann, T. (1937) *Proc. R. Soc. London, Ser. B 122*, 119–133.

Kitagawa, T., & Teraoka, J. (1982) in *The Biological Chemistry of Iron* (Dunford, H. B., et al., Eds.) pp 375–389, Reidel, Dordrecht, The Netherlands.

Kotani, M. (1968) *Adv. Quantum Chem. 4*, 227–266.

LaMar, G. N., Chacko, V. P., & deRopp, J. S. (1982) in *The Biological Chemistry of Iron* (Dunford, H. B., et al., Eds.) pp 357–373, Reidel, Dordrecht, The Netherlands.

Lang, G. (1970) *Q. Rev. Biophys. 3*, 1–60.

Lang, G., Asakura, T., & Yonetani, T. (1969) *J. Phys. C 2*, 2246–2261.

Lang, G., Spartalian, K., & Yonetani, T. (1976) *Biochim. Biophys. Acta 451*, 250–258.

Loew, G. H., & Herman, Z. (1980) *J. Am. Chem. Soc. 102*, 6173–6174.

Maeda, Y., & Morita, Y. (1967) *Biochem. Biophys. Res. Commun. 29*, 680–685.

Maltempo, M. M., & Moss, T. H. (1976) *Q. Rev. Biophys. 9*, 181–215.

Maltempo, M. M., Ohlsson, P. I., Paul, K.-G., Petersson, L., & Ehrenberg, A. (1979) *Biochemistry 18*, 2935–2941.

Moriya, T. (1960) *Phys. Rev. 120*, 91–98.

Moss, T., Ehrenberg, A., & Bearden, A. J. (1969) *Biochemistry 8*, 4159–4162.

Münck, E., Groves, J. L., Tumolillo, T. A., & Debrunner, P. G. (1973) *Comp. Phys. Commun. 5*, 225–238.

Murthy, M. R. N., Reid, T. J., III, Sicignano, A., Tanaka, N., & Rossmann, M. G. (1981) *J. Mol. Biol. 152*, 465–499.

Oosterhuis, W. T., & Lang, G. (1973) *J. Chem. Phys. 58*, 4757–4765.

Orbach, R., & Stapleton, H. J. (1972) in *Paramagnetic Resonance* (Geschwind, S., Ed.) pp 121–216, Plenum Press, New York.

Palcic, M. M., Rutter, R., Araiso, T., Hager, L. P., & Dunford, H. B. (1980) *Biochem. Biophys. Res. Commun. 94*, 1123-1127.
Parak, F., Bade, D., & Marie, A. L. (1979) *J. Phys., Colloq. (Orsay, Fr.) 40*, 528-530.
Penner-Hahn, J. E., McMurry, T. J., Renner, M., Latos-Grazynsky, L., Smith-Eble, K., Davis, I. M., Balch, A. L., Groves, J. T., Dawson, J. H., & Hodgson, K. O. (1983) *J. Biol. Chem. 258*, 12761-12764.
Poulos, T. L., Freer, S. T., Alden, R. A., Edwards, S. L., Skogland, U., Takio, K., Eriksson, B., Xuong, N., Yonetani, T., & Kraut, J. (1980) *J. Biol. Chem. 255*, 575-580.
Ristau, O. (1981) *Period. Biol. 83*, 39-49.
Roberts, J. E., Hoffman, B. M., Rutter, R., & Hager, L. P. (1981a) *J. Biol. Chem. 256*, 2118-2121.
Roberts, J. E., Hoffman, B. M., Rutter, R., & Hager, L. P. (1981b) *J. Am. Chem. Soc. 103*, 7654-7656.
Rutter, R. (1982) Ph.D. Thesis, University of Illinois.
Schonbaum, G. R. (1973) *J. Biol. Chem. 248*, 502-511.
Schonbaum, G. R., & Lo, S. (1972) *J. Biol. Chem. 247*, 3353-3360.
Schulz, C. E. (1979) Thesis, University of Illinois.
Schulz, C., & Debrunner, P. G. (1984) *Biophys. J. 45*, 242a.
Schulz, C., Chiang, R., & Debrunner, P. G. (1979a) *J. Phys., Colloq. (Orsay, Fr.) 40*, C2-534-C2-536.
Schulz, C. E., Devaney, P. W., Winkler, H., Debrunner, P. G., Doan, N., Chiang, R., Rutter, R., & Hager, L. P. (1979b) *FEBS Lett. 103*, 102-105.
Shahangian, S., & Hager, L. P. (1982) *J. Biol. Chem. 257*, 11529-11533.
Shannon, L. M., Kay, E., & Lew, J. Y. (1966) *J. Biol. Chem. 241*, 2166-2172.
Sharrock, M., Debrunner, P. G., Schulz, C., Lipscomb, J. D., Marshall, V., & Gunsalus, I. C. (1976) *Biochim. Biophys. Acta 420*, 8-26.
Simonneaux, G., Scholz, W. F., Reed, C. A., & Lang, G. (1982) *Biochim. Biophys. Acta 716*, 1-7.
Slade, E. F., & Farrow, R. H. (1972) *Biochim. Biophys. Acta 278*, 450-458.
Tamura, M., Osakura, T., & Yonetani, T. (1972) *Biochim. Biophys. Acta 268*, 292-304.
Theorell, H. (1941) *Enzymologia 10*, 250.
Theorell, H. (1942) *Ark. Kemi, Min. Geol. 16A* (2).
Theorell, H., & Ehrenberg, A. (1952) *Arch. Biochem. Biophys. 41*, 442-461.
Tsai, R., Yu, C.-A., Gunsalus, I. C., Peisach, J., Blumberg, W. E., Orme-Johnson, W. H., & Beinert, H. (1970) *Proc. Natl. Acad. Sci. U.S.A. 66*, 1157-1163.
Weger, M. (1960) *Bell Syst. Tech. J. 39*, 1013-1112.
Welinder, K. G. (1979) *Eur. J. Biochem. 96*, 483-502.
Willstätter, R., & Stoll, A. (1918) *Liebigs Ann. Chem. 416*, 21-64.
Willstätter, R., & Pollinger, A. (1923) *Liebigs Ann. Chem. 430*, 269-319.
Winkler, H., Schulz, C., & Debrunner, P. G. (1979) *Phys. Lett. 69A*, 360-363.

Sarcoplasmic Reticulum Adenosinetriphosphatase Phosphorylation from Inorganic Phosphate. Theoretical and Experimental Reinvestigation†

Florent Guillain,* Philippe Champeil,‡ and Paul D. Boyer

ABSTRACT: P_i phosphorylation of sarcoplasmic reticulum (SR) vesicles in the absence of Ca was reinvestigated. Theoretical analysis shows that, for various substrate concentrations, the time dependence of phosphoenzyme formation does not allow determination of an unambiguous reaction scheme or estimation of the stoichiometry of the reaction. To overcome this difficulty, we measured medium P_i oxygen exchange, [^{32}P]-phosphoenzyme formation, and intrinsic fluorescence. We found that contrarily to the usual assumption the substrate binding step in the phosphorylation direction at pH 6.0, KCl = 0, and 23 °C is a slow process whose bimolecular rate constant is around 5×10^3 M^{-1} s^{-1} for both Mg and P_i binding. We confirm [Lacapère, J. J., Gingold, M. P., Champeil, P., & Guillain, F. (1981) *J. Biol. Chem. 256*, 2302-2306] that, in a second step, the establishment of a covalent bond between the bound P_i and the enzyme is formed with a rate constant ≥ 20 s^{-1} whereas the dephosphorylation rate constant is 2-3 s^{-1}. These results imply that under optimal conditions for phosphorylation, the enzyme is almost entirely phosphorylated at concentrations of 20 mM $MgCl_2$ and 20 mM P_i. Study of the phosphorylation reaction under various experimental conditions shows that reduction of the phosphoenzyme level upon KCl addition is mainly due to the augmentation of the hydrolysis rate constant. In addition we propose that the strong inhibition by large amounts of $MgCl_2$ is due to the formation of an $E^?$·Mg complex unfit for phosphorylation by P_i. Diminution of the phosphoenzyme level when the pH increases reflects higher enzyme sensitivity to Mg inhibition at alkaline pH. Results for inhibition by ATP of the phosphorylation reaction at pH 6.0 and KCl = 0 are also presented and discussed in the light of the data available in the literature.

One of the essential characteristics of the SR-ATPase[1] is its ability to function in a forward or a backward direction, i.e., either to accumulate calcium at the expense of ATP hydrolysis or to synthesize ATP from ADP and P_i via a phosphoryl enzyme, at the expense of an outflux of calcium.

† From the Molecular Biology Institute, University of California, Los Angeles, California 90024. *Received January 24, 1984.* Supported by National Science Foundation Grant PCM-81-00817, P. D. Boyer, Principal Investigator.

* Address correspondence to this author at the Département de Biologie, CEN-Saclay, 91191 Gif sur Yvette, France.
‡ Present address: Département de Biologie, CEN-Saclay, 91191 Gif sur Yvette, France.

[1] Abbreviations: SR, sarcoplasmic reticulum; ATPase, adenosinetriphosphatase; EGTA, ethylene glycol bis(β-aminoethyl ether)-*N,N,N',N'*-tetraacetic acid; EDTA, ethylenediaminetetraacetic acid; Mes, 2-(*N*-morpholino)ethanesulfonic acid; Mops, 4-morpholinepropanesulfonic acid; Tris, tris(hydroxymethyl)aminomethane; $\Delta F/F$, relative fluorescence change.

0006-2960/84/0423-4754$01.50/0